Research Article Vol. 28, No. 4 / 17 February 2020 / Optics Express 5507
Optics EXPRESS

Interferometric method for determining the losses of spatially multi-mode nonlinear waveguides based on second harmonic generation.

MATTEO SANTANDREA,[1,*] MICHAEL STEFSZKY,[1] GANAËL ROELAND,[2] AND CHRISTINE SILBERHORN[1]

[1] *Integrated Quantum Optics, Paderborn University, Warburger Straße 100, 33098 Paderborn, Germany*
[2] *Laboratoire Kastler Brossel, Sorbonne Université, CNRS, ENS-PSL Research University, Collège de France, 4 place Jussieu, F-75252 Paris, France*
[*] *matteo.santandrea@upb.de*

Abstract: The characterisation of loss in optical waveguides is essential in understanding the performance of these devices and their limitations. Whilst interferometric-based methods generally provide the best results for low-loss waveguides, they are almost exclusively used to provide characterization in cases where the waveguide is spatially single-mode. Here, we introduce a Fabry-Pérot-based scheme to estimate the losses of a nonlinear (birefringent or quasi-phase matched) waveguide at a wavelength where it is multi-mode. The method involves measuring the generated second harmonic power as the pump wavelength is scanned over the phase matching region. Furthermore, it is shown that this method allows one to infer the losses of different second harmonic spatial modes by scanning the pump field over the separated phase matching spectra. By fitting the measured phase matching spectra from different titanium indiffused lithium niobate waveguides to the model presented in this paper, it is shown that one can estimate the second harmonic losses of a single spatial-mode, at wavelengths where the waveguides are spatially multi-mode.

1. Introduction

Optical waveguides have enabled the expansion of optical networks in a very short time. Naturally, this technology is advancing in order to include, for example, high power, high efficiency and/or quantum applications [1,2]. For the most demanding applications, such as squeezing in fibre networks [3] or on-chip entanglement [4], the losses of the waveguide are of critical importance. Therefore, the reliable characterisation of these losses is a critical issue.

A number of methods for loss characterization and variants of these methods exist. These methods can be categorised into a few broad schemes: cut-back methods, fluorescence/scatter imaging, resonance techniques and optical transmission measures. These various methods perform differently under given circumstances. Interferometric methods tend to have greater precision as the losses decrease and so are more suited for characterisation of low loss waveguides [5–7]. Additionally, these methods generally do not require additional processing steps because the facets' Fresnel reflections can be used for characterisation.

Unfortunately, such resonance-based methods are generally unsuitable in waveguides that are spatially multi-mode for the probe field. This is due to the fact that it is experimentally very difficult to couple light into the waveguide such that only a single propagation-mode of the waveguide is excited. These different spatial modes have disparate dispersion properties, leading to different free spectral ranges (FSRs) for the various spatial modes. The resulting transmitted power will consist of multiple resonance conditions with unknown magnitude and phase, generally making the problem intractable. Under certain conditions the losses can still be obtained from

#380788 https://doi.org/10.1364/OE.380788
Journal © 2020 Received 18 Oct 2019; revised 16 Jan 2020; accepted 16 Jan 2020; published 13 Feb 2020

Optics EXPRESS

such a measurement, but this requires the fulfillment of a number of conditions which are, in general, not satisfied [8]. Alternatively, it may also be possible to use a Fourier decomposition method [9]. Application of this method in multi-mode systems requires that the higher order spatial modes do not couple, a condition that is often met, but also requires moderately high cavity finesses. The second condition makes this method more suitable for systems with high refractive index, such as semiconductor waveguides, where the Fresnel reflection is greater, and is not directly applicable to many waveguiding platforms such as lithium niobate.

For this reason, devices implementing multi-colour processes, such as difference or sum-frequency generation, typically have their losses characterised at the longest wavelength, where the waveguide is single-mode. This value is often used to estimate or bound the losses at shorter wavelengths. However, one cannot know *a priori* the exact relationship between the losses at different wavelengths. This is problematic when the losses at the shorter wavelengths are critical, for example in frequency converters that aim to produce a field close to the transparency cut-off region of a particular material [10].

Here we present a method for loss characterisation in such systems by measuring the phase matching spectrum of the second harmonic (SH) process as the pump (fundamental) wavelength is varied over the phase matching spectrum. The resulting phase matching spectrum is compared to theory in order to estimate the losses of the second harmonic field. Additionally, this method allows one to probe the second harmonic losses for any second harmonic spatial mode whose corresponding phase matching spectrum can be probed with the given pump field. The approach is quite general and can be applied to both birefringent and quasi-phase matched systems. One could extend the theory to other processes such as sum frequency generation and type II second-harmonic generation processes.

2. Measurement strategy and theory

In the standard low-finesse Fabry-Pérot loss measurement the power transmitted through a waveguide is recorded when scanning a probe field over wavelengths where the system is single-mode [5]. Given that one knows the reflectance of the end facets to a high precision, the interference effects observed in the transmitted power can be used to determine the losses inside the resonator at the same wavelength as the probe field.

The general strategy employed in the method presented here is that, in addition to first determining the losses at the fundamental wavelength using the standard method, we also measure the interferometric fringing that one observes in the generated second harmonic field when scanning the pump over the wavelengths where phase matching occurs. One can then fit the obtained phase matching spectrum to a model of this system and gain information about the losses of the second harmonic field. A single spatial-mode for the second harmonic field is guaranteed due to the fact that the single-mode pump field is phasematched to only a single second harmonic spatial-mode over the wavelength region of interest. The unique dispersion properties of different spatial modes generally ensures that this is the case.

The system is modeled using an extension of the second harmonic generation theory presented by Berger [11]. In this method, the internal second harmonic fields are first described and thereafter solved simultaneously in order to find a self-consistent cavity solution. In order to arrive at an analytic expression it is assumed that the pump field, at the fundamental frequency, is not depleted by the nonlinear process. This assumption is trivial to establish experimentally by correctly choosing the power in the pump field. It may be possible to remove this restriction by considering a numerically based iterative approach [12]. However, this will further complicate the treatment and will not provide an analytic expression.

Optics EXPRESS

The circulating fundamental field *amplitude* travelling in the cavity in the forward direction $E^f_\omega(0)$ is given by the usual Fabry-Pérot resonance condition

$$E^f_\omega(0) = E_{in}\frac{\tau_{\omega,0}}{1-\rho_{\omega,0}\rho_{\omega,L}\cdot \mathrm{e}^{-i2k_\omega L}\cdot \mathrm{e}^{-\alpha_\omega L}} \tag{1}$$

where k_ω $[m^{-1}]$ is the wavevector of the fundamental field, α_ω $[m^{-1}]$ are the intensity losses for the fundamental field, $\rho_{\omega,0/L}$ is the complex reflectivity for the input/output facet at ω and $\tau_{\omega,0}$ is the complex transmission of the input facet at ω. Note that from these definitions one can also express the circulating fundamental field *amplitude* travelling in the backwards direction, $E^b_\omega(L) = \rho_{\omega,L}E_\omega \mathrm{e}^{ik_\omega L}$.

With the non-pump depletion approximation, the generated second harmonic field *amplitude* can be calculated from [12] as

$$\frac{\mathrm{d}E_{2\omega}}{dz} = i\gamma[E_\omega \mathrm{e}^{-\alpha_\omega z/2}]^2 \mathrm{e}^{i\Delta k z} - \frac{\alpha_{2\omega}}{2}E_{2\omega}, \tag{2}$$

where $E_{\omega/2\omega}(z)$ is the fundamental/second harmonic field amplitude at position z, $\alpha_{2\omega}$ $[m^{-1}]$ represents the (intensity) losses of the second harmonic field, γ $[m/V]$ is the nonlinear coupling coefficient determining the strength of the nonlinear process, the wave vector mismatch between the fundamental and second harmonic field is defined by $\Delta k = 2k_\omega - k_{2\omega} + k_{QPM}$ $[m^{-1}]$, and $k_{2\omega}$ $[m^{-1}]$ is the wave vector of the second harmonic field. The term $k_{QPM} = 2\pi/\Lambda$ is required only when analysing periodically poled structures, with period Λ. Note that the effect of losses in the fundamental field in Eq. (2) have been included by considering a spatially dependent fundamental amplitude in the form $E_\omega \mathrm{e}^{-\alpha_\omega z/2}$.

Integration of Eq. 2 with initial conditions $(E_\omega(z_0), E_{2\omega}(z_0))$ over a crystal length L yields the component of the second harmonic amplitude after passing through the length z due to the nonlinear interaction

$$E_{2\omega}(z) = SH_z\left(E_\omega(z_0), E_{2\omega}(z_0)\right), \tag{3}$$

$$= 2i\gamma\frac{\mathrm{e}^{(\alpha_{2\omega}-2\alpha_\omega+2i\Delta k)z/2}-1}{\alpha_{2\omega}-2\alpha_\omega+2i\Delta k}E^2_\omega \mathrm{e}^{-\alpha_{2\omega}z/2} + E_{2\omega}\mathrm{e}^{-\alpha_{2\omega}z/2}. \tag{4}$$

To derive an expression for the circulating second harmonic field amplitude, one defines the second harmonic field *amplitudes* travelling in the forward direction at the left and right sides of the sample, $E^f_{2\omega}(0)$ and $E^f_{2\omega}(L)$, and in the backwards direction at the left and right sides of the sample, $E^b_{2\omega}(0)$ and $E^b_{2\omega}(L)$, respectively, as illustrated in Fig. 1. The relation between these four amplitudes can be described by the following system:

$$E^f_{2\omega}(L) = SH_L\left(E^f_\omega(0), E^f_{2\omega}(0)\right)e^{ik_{2\omega}L}, \tag{5}$$

$$E^b_{2\omega}(L) = \rho_{2\omega,L}E^f_{2\omega}(L), \tag{6}$$

$$E^b_{2\omega}(0) = SH_L\left(E^b_\omega(L), E^b_{2\omega}(L)\right)e^{ik_{2\omega}L}, \tag{7}$$

$$E^f_{2\omega}(0) = \rho_{2\omega,0}E^b_{2\omega}(0), \tag{8}$$

where $E^b_\omega(L) = \rho_{\omega,L}E^f_\omega(0)\mathrm{e}^{-ik_\omega L}\mathrm{e}^{-\alpha_\omega L/2}$. The total circulating second harmonic field at steady-state can be found by simultaneously solving these equations, thereby ensuring self-consistency of the SH field amplitude.

Optics EXPRESS

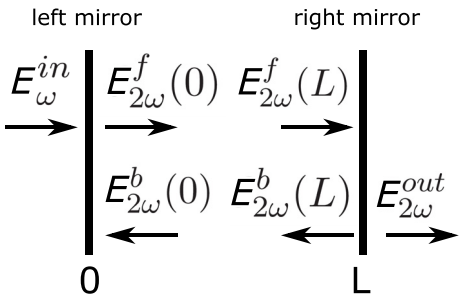

Fig. 1. Sketch detailing the forward and backward propagating waves used for the theoretical treatment of the waveguide resonator.

Solving this set of equations, propagating through the right side mirror in order to find the second harmonic field exiting the cavity and substituting (1) we find the output second harmonic field amplitude as

$$\begin{aligned} E_{2\omega}^{out} &= \tau_{2\omega,L} E_{2\omega,L}^f \\ &= \tau_{2\omega,L}\gamma (E_\omega^{in})^2 \frac{\tau_{\omega,0}^2}{(1-\rho_{\omega,0}\rho_{\omega,L}\mathrm{e}^{-2ik_\omega L-\alpha_\omega L})^2}\times \\ &\quad iL\mathrm{sinc}\left(\frac{(\Delta k - i\alpha_{2\omega}/2 + i\alpha_\omega)L}{2}\right)\mathrm{e}^{\frac{(\Delta k - i\alpha_{2\omega}/2+i\alpha_\omega)L}{2}}\times \\ &\quad \frac{1}{1-\rho_{2\omega,0}\rho_{2\omega,L}\mathrm{e}^{-i2k_{2\omega}L-\alpha_{2\omega}L}}\times \\ &\quad \left(1+\rho_{2\omega,0}\rho_{\omega,L}^2\mathrm{e}^{-ik_{2\omega}L}\mathrm{e}^{-i2k_\omega L}\mathrm{e}^{-\alpha_{2\omega}L/2-\alpha_\omega L}\right)\mathrm{e}^{-\alpha_{2\omega}L/2-ik_{2\omega}L}. \end{aligned} \tag{9}$$

This equation is split into four terms in order to highlight the factors that contribute to the observed interference fringes, as noted by Berger [11]. The first term represents the Fabry-Pérot interference of the fundamental field; the second term is the spectrum of the second harmonic signal generated in a single pass; the third term is the Fabry-Pérot interference of the second harmonic field and the final term represents the phase mismatch between the nonlinear polarization and the second harmonic field over half of a cavity round trip, or equivalently, the phase between the forward and backwards propagating second harmonic waves.

The second harmonic power exiting the system when pumped at wavelength λ is then given by squaring the field (9), $I_{2\omega}(\lambda) = |E_{2\omega}^{out}(\lambda)|^2$.

The profile of $I_{2\omega}(\lambda)$ depends on the complex facet reflectivities $\rho = |\rho|\mathrm{e}^{i\phi}$ at $z = 0$ and $z = L$, the fundamental and SH losses $\alpha_{\omega/2\omega}$, on the cavity length L and on the poling period Λ, if present. Qualitatively, one can observe that these parameters affect the shape of $I_{2\omega}(\lambda)$ in different ways: the length L of the sample affects the width of the spectrum and the free spectral range (FSR) of the primary frequency component of the fringing, the contrast of the fringes depends on the magnitude of both the fundamental and second harmonic losses and the complicated internal structure of the fringing is dependent on the facet reflectivities and the crystal length. However, due to the three different phase factors present in Eq. (9), the shape of the fringes of the phase matching spectrum changes dramatically within the main phase matching peak. This problem is revealed in Fig. 3, where it can be seen that the different phases found for the two spatial modes leads to interference fringes with very different symmetry and structure of the interference envelope. Therefore, the contrast of the interference fringes is somewhat ill-defined for the given data. Because of this, a new approach is required. In the following section it is shown that it

Optics EXPRESS

is possible to find an optimized fit to these free variables, thereby providing an estimate of the value of $\alpha_{2\omega}$.

3. Fitting procedure

The fit of the theory to the measured data is undertaken in steps in order to constrain the range of some of the parameters to physically acceptable values. First, both the model $I_{2\omega}(\lambda)$ and the measured data $I_{meas}(\lambda)$ are normalized to have unitary maximum intensity. Next, the loss of the fundamental field α_ω is fixed to the value measured using the standard low-finesse loss technique [5]. This measurement is performed scanning the fundamental field over wavelengths slightly shifted away from phase matching so that the second harmonic process does not influence the measurement. Next, the initial estimate L_0 of the sample length is retrieved from the free spectral range of the fundamental field. In particular, by Fourier transforming $I_{meas}(\lambda)$, the optical path length of the resonator is estimated from the FSR of the primary frequency components, corresponding to the interference of the fundamental field (1). From this value, the initial estimate L_0 of the waveguide physical length can be inferred, without requiring additional measurements. Finally, an initial estimate Λ_0 for the poling period is retrieved from the central phase matching wavelength λ_{pm}, estimated from the data using a weighted average of the recorded wavelengths, where the second harmonic spectral intensity is used as weights. The retrieved Λ_0 is close to the value defined during the lithography step but varies slightly since it absorbs small errors in the refractive index models available.

After determining the center values of these parameters, the theoretical phase matching spectrum $I_{2\omega}(\lambda)$ is then fitted to the measured data $I_{meas}(\lambda)$. At this stage, there are a total of 9 free parameters that determine the shape of the SH intensity $I_{2\omega}(\lambda)$, namely four reflectivity amplitudes $|\rho|_{\omega/2\omega,0/L}$, four reflectivity phases $\phi_{\omega/2\omega,0/L}$ and $\alpha_{2\omega}$. One can theoretically constrain the facet complex reflectivities to those estimated using Fresnel coefficients, as is done when estimating the fundamental losses α_ω; however, leaving them as a free parameter of the fit provides a check for the quality of the end facets. If the reflection coefficients converge to the expected values, as was observed for all investigated waveguides, this provides confidence that the end facets are of high quality, validating the retrieved values for the fundamental losses α_ω. Prior to the final fit, it is helpful to find a first estimate for the phases ϕ, to avoid the fitting procedure becoming stuck in a local minimum. For this reason, the phases ϕ are first optimised assuming $|\rho|_{\omega/2\omega,0/L}$ as given by the Fresnel coefficients, and $\alpha_{2\omega} = \alpha_\omega$ as a rough estimate of what one might expect to find for the second harmonic losses. The phases ϕ thusly retrieved are used as initial parameters in the second step of the fit, where the model $I_{2\omega}(\lambda)$ is fitted again to the measured data. At this stage, the length L, the poling period Λ, the second harmonic losses $\alpha_{2\omega}$, the modules and phases of the facet reflectivities $\rho_{\omega/2\omega,0/L}$ are considered as fitting parameters. The length L is constrained to a 500μm range around L_0, the poling period Λ is constrained to be within 1% of Λ_0, while the phases retrieved in the first step of the optimisation are used as initial parameters for the fitting algorithm.

The fitting routine solves a nonlinear least square minimisation problem using the Trust Region Reflective algorithm that minimizes the mean squared error (MSE) between the model $I_{2\omega}(\lambda)$ and the data $I_{meas}(\lambda)$. Due to the complexity of the model, the initial values for the reflectivities of the facets and $\alpha_{2\omega}$ are initialised with random weights and the minimisation is repeated 10 times to find the best set of parameters. To obtain physically meaningful results, we bound the parameters of the fit during the minimisation. In particular, the phases of ρ are constrained between $[0,2\pi]$ and the reflectivities are permitted to vary by a few percent from the calculated values obtained by the Fresnel equation. Moreover, as some measured spectra showed asymmetries attributable to waveguide inhomogeneities [13], only the central lobe of the second harmonic spectrum was used during the fit.

Optics EXPRESS

Note that the length and the poling period are allowed to vary slightly in this fit in order allow some flexibility, required due to phase matching distortions in the measured data. Furthermore, the mirror reflectivities are treated as complex numbers in order to account for an unknown phase shift on reflection at the end facets of the sample. This phase shift can be extended in order to include the unknown phase shifts present in a quasi-phase matched sample. In such samples the length of the first and final domains are generally unknown and will impart an unknown phase shift on the two fields, which can be absorbed by the phase term in the complex reflectivities.

As a final note, the model presented in Eq. (9) requires the refractive indices of both the fundamental and second harmonic fields as the fundamental pump field is varied - the Sellmeier equation. For the titanium-indiffused lithium niobate waveguides investigated here these dispersion relations have been calculated using a finite element solver written in Python implementing the model described in [14]. This model provides a very accurate description of the dispersion, with a predicted poling period within 0.25μm of the nominal one (1% error). In contrast, the bulk model for lithium niobate crystals [15] predicts poling periods 1.3μm away from the nominal ones (8% error).

4. Results

We apply the described measurement technique in order to retrieve the SH losses of a 31.2mm long 7μm-wide titanium indiffused waveguide designed for single spatial-mode operation in the 1450nm-1600nm wavelength band. The system utilises a 16.8 μm poling period to achieve type 0 quasi-phase matching for second harmonic generation in the TM00 spatial mode when pumped with a fundamental field at 1525nm. This system also supports second harmonic generation in the TM01 mode with a pump field at 1480nm. The losses α_ω of each of these phase matching processes at the fundamental wavelength are first found slightly off phase matching. At around 1525nm the fundamental field losses were found to be 0.21 ± 0.04 dB/cm and at around 1481nm the losses were found to be 0.24 ± 0.07 dB/cm. The losses at the second harmonic wavelength were bounded by performing a simple transmission measurement of a 760nm field. The ratio of the power exiting the coated outcoupling lens to the power entering the coated incoupling lens reveals that the total coupling and waveguide losses were less than ~3.0 dB/cm, taking into account the effect of the Fabry-Pérot resonance due to the Fresnel reflections of the polished end-facets.

Subsequently, the phase matching spectra of the second harmonic field are recorded as the fundamental wavelength is scanned over the phase matching profile for the TM00 and TM01 second harmonic modes, using the setup shown in Fig. 2. The measured phase matching spectra and the fits found using the procedure described in the previous section are illustrated in Fig. 3a.

An excellent qualitative fit between the measured profile and the theory is observed. The frequency of the fringing and the envelope of this central region overlap well. In particular, the insets show zoomed-in regions of the fits that highlight the fact that even the highly complex structure of the interferences is reproduced by the theory. It can be seen, however, that the presence of waveguide imperfections affects the fit of the "side lobes" of the profile. This effect is particularly relevant for the TM00 mode, as can be seen from Fig. 3. The reason is that the dispersion of the TM00 is more sensitive to waveguide variations than the higher order modes for the waveguides under consideration. The minimisation routine results in losses of 1.2± 0.2 dB/cm for the TM00 second harmonic mode and losses of 1.3± 0.1 dB/cm for the TM01 mode, where the errorbar have been derived considering a 1% variation of the MSE.

In order to check the validity of the fit, in particular the performance of the chosen minimisation routine, we also show the variation of the MSE for both of these fits as the second harmonic losses are varied, holding all other parameters constant. The MSE's found in this way are illustrated in Fig. 4.

Optics EXPRESS

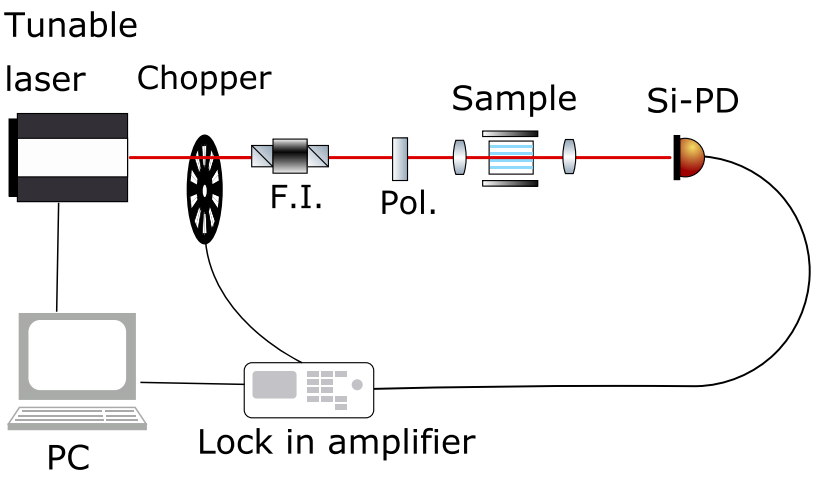

Fig. 2. Setup for the measurement of the second harmonic. The light from an IR laser tunable in the range 1460nm-1640nm (EXFO TUNICS) passes through a chopper used in conjuction with a lock-in amplifier to enhance the second harmonic readout. The IR field then passes through a Faraday isolator (F.I.) that suppresses any backreflection from the sample. A polariser is used in front of the sample to set the input polarisation of the fundamental field. Anti-reflection (AR) coated 8mm focal length aspheric lenses are used for the in- and out-coupling. Finally, the second harmonic light is measured via a silicon photodiode connected to a lock-in amplifier.

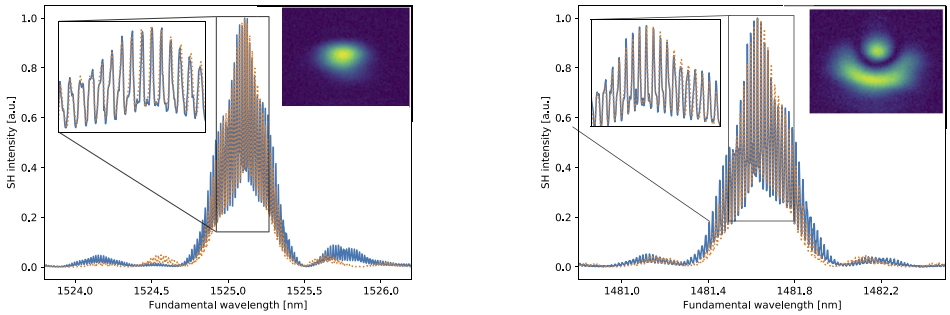

(a) TM00 (b) TM10

Fig. 3. Measured (blue line) and theoretical fit (orange dotted) for the TM00 and TM10 second harmonic spatial mode phase matching spectra. The insets in the top right show the measured intensity distributions of these spatial modes, while the insets in the top left show a zoom-in on the central lobe.

The fitting technique employed here is highly sensitive to the shape of the MSE as a function of $\alpha_{2\omega}$. In particular, the MSE must exhibit a global minimum for the fit to converge to a reasonable value for the SH losses, as is the case for the waveguide analysed in Figs. 3 and 4.

However, a global minimum for the MSE was not always observed. This was seen when investigating a 10mm long waveguide from a second 7μm-wide titanium indiffused waveguide. The process under investigation was again a quasi-phase matched, type 0 second harmonic generation in the TM00 spatial mode with Λ=16.8 μm. This waveguide was found to have losses α_{ω}=0.20±0.04 dB/cm near to the phase matching wavelength of 1527nm. As was done for the longer sample, a field transmission measurement was used to bound the losses of the tested

Optics EXPRESS

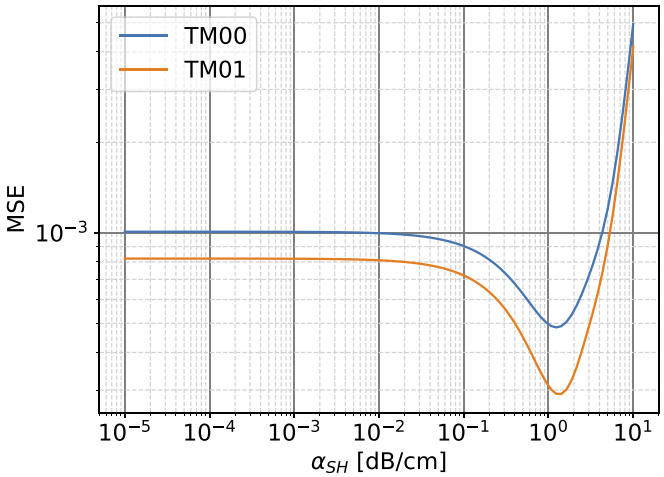

Fig. 4. Mean squared error of the sum squared residuals between the model and the data for the TM00 and TM01 second harmonic spatial modes.

waveguides at 760nm to less than ~2.5 dB/cm. Using the method described in the previous section, the fit yielded vanishingly small (below 10^{-4} dB/cm) second harmonic losses.

Although the second harmonic losses inferred from the minimum of the MSE provided unphysical results, we show that it is nevertheless still possible to find an upper bound for the second harmonic losses. The behaviour of the MSE is again investigated by varying the second harmonic losses $\alpha_{2\omega}$ in the resulting fit while holding all other parameters constant. The MSE obtained as the second harmonic losses are varied is shown in Fig. 6, while the resulting modified fits for a select number of second harmonic loss values are illustrated in Fig. 5. In contrast to the previously investigated waveguide, the MSE for this waveguide does not show a global minimum. Instead, the MSE asymptotes to some value at low second harmonic losses and begins to increase rapidly for second harmonic losses greater than 0.3 dB/cm. Figure 5 shows this behaviour in more detail. The modified fit reproduces the measured interference fringes with losses up to $\alpha_{2\omega} \lesssim 0.1$ dB/cm, while the modified fit becomes noticeably worse with high second harmonic loss values of 10 dB/cm. An upper bound on the second harmonic losses can thus be found by choosing a threshold value in relation to the asymptote in the MSE. For example, setting a 10% threshold for the variation of the MSE with respect to its minimum value provides an upper bound of $\alpha_{2\omega} \leq 0.35$ dB/cm for the second harmonic losses in this waveguide. This result and the previously determined losses for the first waveguide are summarised in Table 1.

Table 1. Measured loss values of waveguide 1 (WG1) and waveguide 2 (WG2).

SH spatial mode	WG1 TM00	WG1 TM01	WG2 TM00
Fund. Loss	0.21±0.04dB/cm	0.24±0.07dB/cm	0.20±0.04dB/cm
Harm. Loss	1.2±0.2dB/cm	1.3±0.1dB/cm	≤ 0.35dB/cm

It is unclear why a global minimum for the MSE is not found in certain cases. Numerical investigations have shown that the presence of a global minimum in the MSE is mostly correlated to the overall propagation losses of the second harmonic field inside the resonator. In general, it is possible to observe a global minimum for waveguides with second harmonic losses above 0.5-1 dB. At the same time, these numerical simulations show almost no correlation between the the presence of the global minimum and the facet reflectivities or sample length. It is likely that the chosen cost function is not sufficiently sensitive to small changes in the second harmonic losses,

Optics EXPRESS

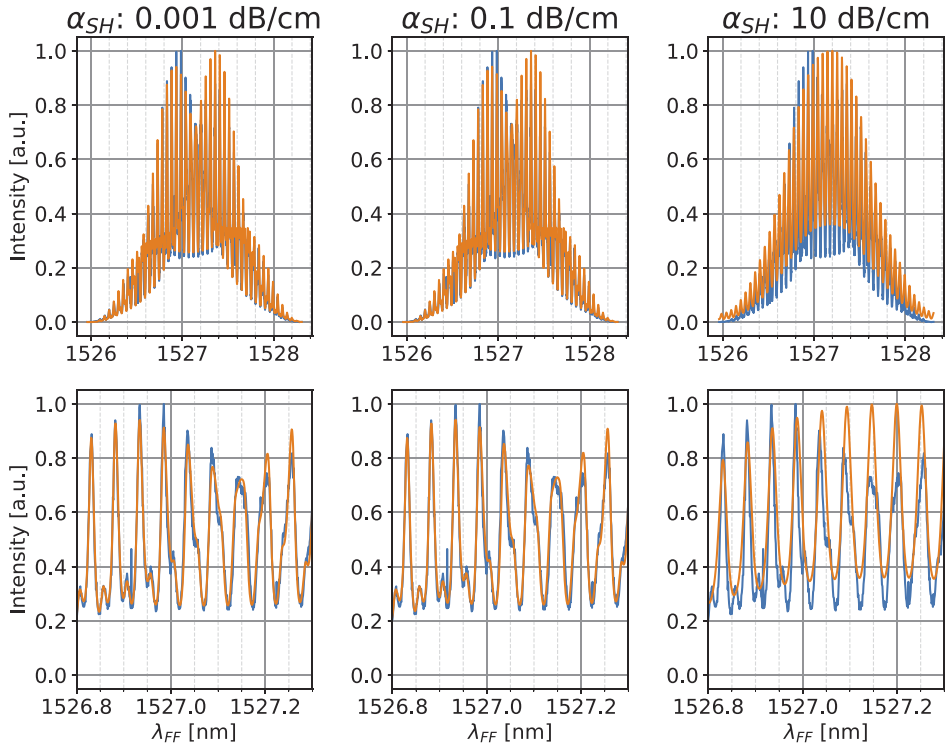

Fig. 5. Central portion of the measured (blue) and fitted (orange) phase matching profiles. It can be qualitatively seen that the fit works very well for low losses but that both the structure and envelope of the fit for higher second harmonic losses is degraded. The bottom row shows a zoom-in on the region around 1527.2nm, highlighting the ability of the model to fit the fine structure of the measured spectrum.

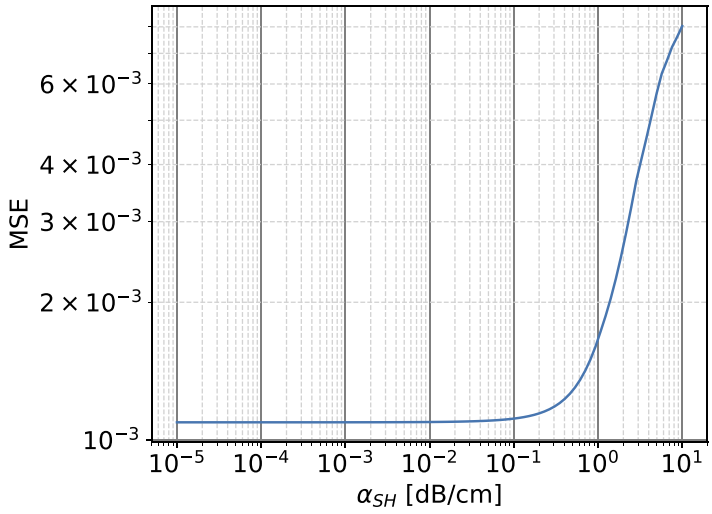

Fig. 6. Mean squared error between the measured and fitted central portion of the phase matching profiles as the second harmonic losses are increased. It can be clearly seen that the mean squared error increases rapidly with losses greater than ~0.1 dB/cm. Of note is that the mean squared error does not increase with vanishingly small second harmonic losses.

Optics EXPRESS

particularly in the presence of experimental imperfections. A more advanced fitting scheme or a different cost function may be able to predict the second harmonic losses with reduced uncertainty, but this is left as future work.

Finally, we characterised several additional waveguides in both samples to certify the validity of the presented method. In particular, we estimated the losses of the TM00 mode in six waveguides

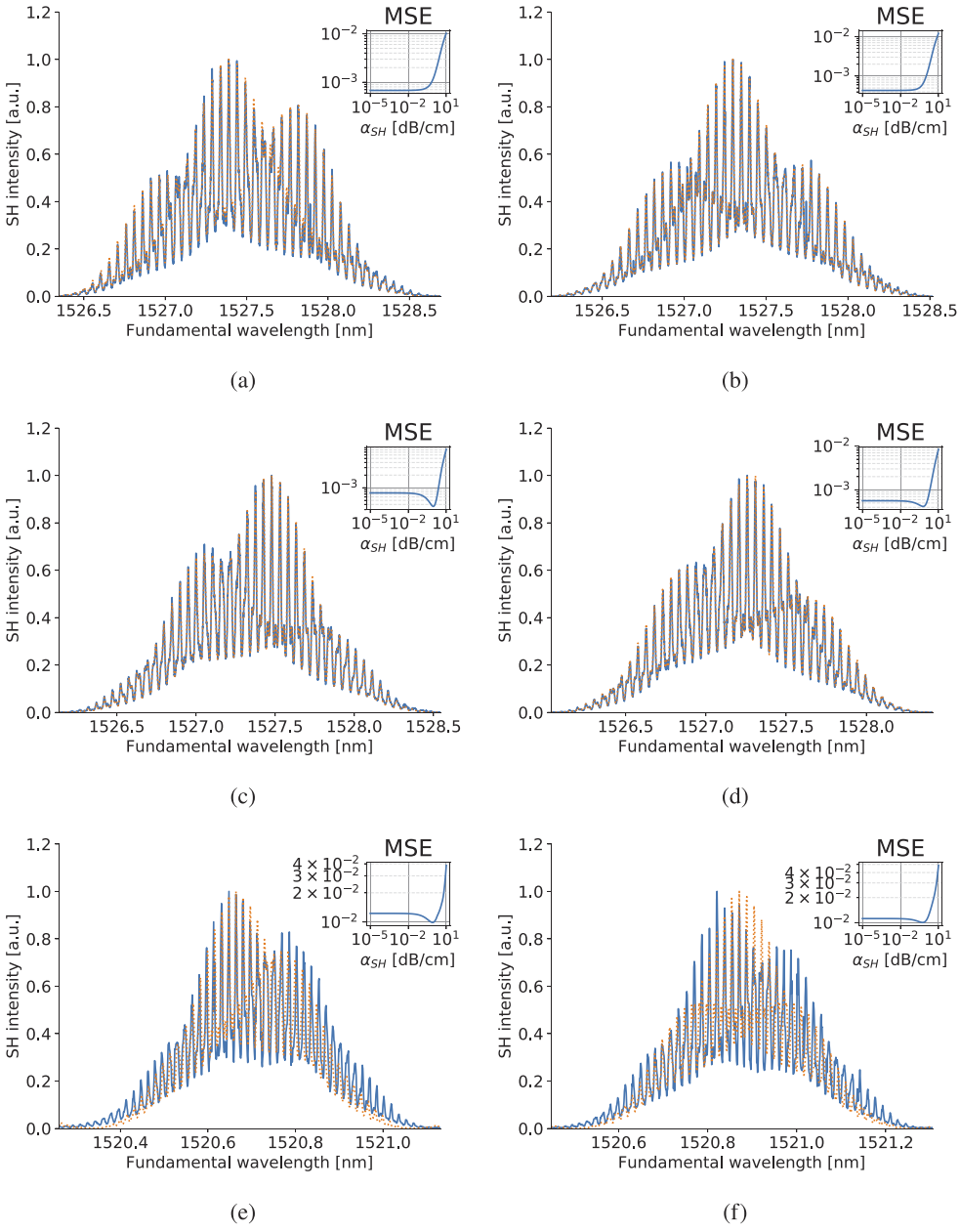

Fig. 7. Fitted phase matching spectra and relative MSE for the TM00 mode of a subset of the measured waveguides. Figures (a)-(d) correspond to 1cm-long waveguides, while Figures (e)-(f) correspond to 3cm-long waveguides. The inferred losses are reported in Table 2.

Optics EXPRESS

in the 1cm-long sample and the losses of both TM00 and TM01 modes in eight waveguides in the 3cm-long sample. Of the twenty-two measured spectra, fourteen show very good agreement between the fitted spectrum and the measured one. A subset of these measurements can be seen in Fig. 7, and the related losses are reported in Table 2. The quality of the fit is different for the 1cm- and the 3cm-long waveguides. On the one hand, the fits of the 1cm-long waveguides always show an excellent agreement with the measured data, even though a minimum for the MSE was not always found. Preliminary investigations reveal that this is likely due to a low value of the propagation losses, as discussed in the previous paragraph. On the other hand, the fits of the 3cm-long waveguides always yield an MSE with a clear global minimum. However, the fitted spectra do not always follow the measured ones, as can be seen from the example in Fig. 5. Preliminary investigations show that this is caused by attempting to fit to a distorted phase matching curve, which are caused by the presence of waveguide inhomogeneities.

Table 2. Measured losses for the fundamental and second harmonic field of the spectra shown in Fig. 7.

WG	(a)	(b)	(c)	(d)	(e)	(f)
L	1cm	1cm	1cm	1cm	3cm	3cm
α_{FF} [dB/cm]	0.38±0.04	0.4±0.1	0.41±0.09	0.12±0.02	0.37±0.07	0.14±0.05
α_{SH} [dB/cm]	≤0.23	≤0.23	0.9±0.1	0.61±0.09	0.8±0.2	0.6±0.2

For waveguides (a) and (b), the upper bounds for α_{SH} have been estimated considering a 10% variation of MSE with respect to its minimum.

5. Conclusion

In this paper we have introduced a new method for characterizing the loss of spatially multi-mode waveguides. A model is introduced that describes the expected phase matching spectrum of the generated second harmonic power, including interferences due to the Fabry-Pérot effect from the uncoated end facets. Experimental data is obtained by scanning the wavelength of the fundamental pump field over the phase matching spectrum corresponding to a chosen, single spatial-mode of the second harmonic field. In this way it is possible to determine the losses of a chosen spatial-mode of the second harmonic. The presented technique is then applied to fourteen waveguides of different lengths. For the 1cm-long waveguides, the fitting routine is able to match the measured SH spectra, even though it provides only an upper bound for the SH losses. For the 3cm-long waveguides, it finds a reasonable estimate of the SH losses, but the quality of the fit is lower, due to distortions of the phase matching spectra. The presented approach is very general and can be extended to other nonlinear processes in virtually any high quality waveguide system.

Funding

Horizon 2020 Framework Programme - UNIQORN (820474); Deutsche Forschungsgemeinschaft (SI 1115/6-1).

Disclosures

The authors declare no conflicts of interest.

References

1. M. Stefszky, R. Ricken, C. Eigner, V. Quiring, H. Herrmann, and C. Silberhorn, "Waveguide cavity resonator as a source of optical squeezing," Phys. Rev. Appl. **7**(4), 044026 (2017).
2. M. Stefszky, V. Ulvila, Z. Abdallah, C. Silberhorn, and M. Vainio, "Towards optical frequency comb generation in continuous-wave pumped titanium indiffused lithium niobate waveguide resonators," Phys. Rev. A **98**(5), 053850 (2018).

Optics EXPRESS

3. F. Kaiser, B. Fedrici, A. Zavatta, V. D'Auria, and S. Tanzilli, "A fully guided-wave squeezing experiment for fiber quantum networks," Optica **3**(4), 362–365 (2016).
4. D. Barral, N. Belabas, L. M. Procopio, V. D'Auria, S. Tanzilli, K. Bencheikh, and J. A. Levenson, "Continuous-variable entanglement of two bright coherent states that never interacted," Phys. Rev. A **96**(5), 053822 (2017).
5. R. Regener and W. Sohler, "Loss in low-finesse Ti:LiNbO$_3$ optical waveguide resonators," Appl. Phys. B **36**(3), 143–147 (1985).
6. K. H. Park, M. W. Kim, Y. T. Byun, D. Woo, S. H. Kim, S. S. Choi, Y. Chung, W. R. Cho, S. H. Park, and U. Kim, "Nondestructive propagation loss and facet reflectance measurments of GaAs/AlGaAs strip-loaded waveguides," J. Appl. Phys. **78**(10), 6318–6320 (1995).
7. D. Clark and M. S. Iqbal, "Simple extension to the fabry-pérot technique for accurate measurement of losses in semiconductor waveguides," Opt. Lett. **15**(22), 1291 (1990).
8. A. De Rossi, V. Ortiz, M. Calligaro, L. Lanco, S. Ducci, V. Berger, and I. Sagnes, "Measuring propagation loss in a multimode semiconductor waveguide," J. Appl. Phys. **97**(7), 073105 (2005).
9. D. Hofstetter and R. L. Thornton, "Theory of loss measurements of Fabry–Perot resonators by Fourier analysis of the transmission spectra," Opt. Lett. **22**(24), 1831 (1997).
10. H. Rütz, K.-H. Luo, H. Suche, and C. Silberhorn, "Towards a quantum interface between telecommunication and UV wavelengths: Design and classical performance," Appl. Phys. B **122**(1), 13 (2016).
11. V. Berger, "Second-harmonic generation in monolithic cavities," J. Opt. Soc. Am. B **14**(6), 1351–1360 (1997).
12. M. Fujimura, T. Suhara, and H. Nishihara, "Theoretical analysis of resonant waveguide optical second harmonic generation devices," J. Lightwave Technol. **14**(8), 1899–1906 (1996).
13. M. Santandrea, M. Stefszky, V. Ansari, and C. Silberhorn, "Fabrication limits of waveguides in nonlinear crystals and their impact on quantum optics applications," New J. Phys. **21**(3), 033038 (2019).
14. E. Strake, G. P. Bava, and I. Montrosset, "Guided Modes of Ti:LiNbO3 Channel Waveguides: A Novel Quasi-Analytical Technique in Comparison with the Scalar Finite-Element Method," J. Lightwave Technol. **6**(6), 1126–1135 (1988).
15. D. Jundt, "Temperature-dependent Sellmeier equation for the index of refraction, n(e), in congruent lithium niobate," Opt. Lett. **22**(20), 1553–1555 (1997).